Rapid and inexpensive fabrication of terahertz electromagnetic bandgap structures

Ziran Wu[1], J. Kinast[2], M. E. Gehm[2], and Hao Xin[1, 2]*

[1]*Department of Physics, University of Arizona, Tucson AZ 85719, USA*
[2]*Department of Electrical and Computer Engineering, University of Arizona, Tucson AZ 85721, USA*
**Corresponding author: hxin@ece.arizona.edu*

Abstract: Modern rapid prototyping technologies are now capable of build resolutions that allow direct fabrication of photonic structures in the GHz and THz frequency regimes. To demonstrate this, we have fabricated several structures with 3D electromagnetic bandgaps in the 100-400 GHz range. Characterization of these structures via THz Time-domain Spectroscopy (THz-TDS) shows very good agreement with simulation, confirming the build accuracy of the approach. This rapid and inexpensive 3-D fabrication method may be very useful for a variety of potential THz applications.

OCIS codes: (050.5298) Photonic crystals; (050.6624) Subwavelength structures; (050.6875) Three-dimensional fabrication; (220.4000) Microstructure fabrication.

References and links

1. P. H. Siegel, "Terahertz technology," IEEE Trans. Microwave Theory Tech. **50**, 910-928 (2002).
2. P. H. Siegel, "Terahertz technology in biology and medicine," IEEE Trans. Microwave Theory Tech. **52**, 2438-2447 (2004).
3. B. Ferguson and X. C. Zhang "Material for Terahertz science and technology," Nat. Mater. **1**, 26-33 (2002).
4. P. de Maagt, R. Gonzalo, Y. C. Vardaxoglou, and J.-M. Baracco, "Electromagnetic band gap antennas and components for microwave and submillimeter wave applications," IEEE Trans. Antennas Propag. **51**, 2667-2677 (2003).
5. E. Yablonovitch, "Inhibited spontaneous emission in solid-state physics and electronics," Phys. Rev. Lett. **58**, 2059-2062 (1987).
6. H. Xin, Z. Wu, A. Yound, and R. Ziolkowski, "THz thermal radiation enhancement using electromagnetic crystals," IEEE AP-S Intl Symp. Dig., 2249-2252 (2007).
7. Z. Lu, S. Shi, J. A. Murakowski, G. J. Schneider, C. A. Schuetz, and D. W. Prather, "Experimental demonstration of self-collimation inside a three-dimensional photonic crystal," Phys. Rev. Lett. **96**, 173902-173905 (2006).
8. B. Martinez, I. Ederra, R. Gonzalo, B. Alderman, L. Azcona, P. G. Huggard, B. D. Hon, A. Hussain, S. R. Andrews, L. Marchand, and P. de Maagt, "Manufacturing tolerance analysis, fabrication, and characterization of 3-D submillimeter-wave electromagnetic-band gap crystals," IEEE Trans. Microwave Theory Tech. **55**, 672-681 (2007).
9. R. Gonzalo, B. Martinez, C. M. Mann, H. Pellemans, P. H. Bolivar, and P. de Maagt "A low-cost fabrication technique for symmetrical and asymmetrical layer-by-layer photonic crystals at submillimeter-wave frequencies," IEEE Trans. Microwave Theory Tech. **50**, 2384-2392 (2002).
10. E. Özbay, E. Michel, G. Tuttle, R. Biswas, K. M. Ho, J. Bostak, and D. M. Bloom, "Terahertz spectroscopy of three-dimensional photonic bandgap crystals," Opt. Lett. **10**, 1155–1157 (1994).
11. F. Laermer and A. Urban, "Challenges, developments and applications of silicon deep reactive ion etching," Microelectron. Eng. **67 - 68**, 349–355 (2003).
12. G. Kiriakidis and N. Katsarakis, "Fabrication of 2-D and 3-D photonic band-gap crystals in the GHz and THz regions," Mater. Phys. Mech. **1,** 20-26 (2000).
13. B. Liu, X. Gong, and W. J. Chappell, "Applications of layer-by-layer polymer stereolithography for three-dimensional high-frequency components," IEEE Trans. Microwave Theory Tech. **52**, 2567-2575 (2004).
14. K. F. Brakora, J. Halloran, and K. Sarabandi, "Design of 3-D monolithic MMW antennas using ceramic stereolithography," IEEE Trans. Antennas Propag. **55**, 790-797 (2007).
15. V. K. Varadan, X. Jiang, and V. V. Varadan, *Microstereolithography and Other Fabrication Techniques for 3D MEMS* (Wiley, Chichester, U.K., 2001).
16. N. Delhote, D. Baillargeat, S. Verdeyme, M. Thevenot, C. Delage, and C. Chaput, "Large experimental bandpass waveguide in 3D EBG woodpile manufactured by layer-by-layer ceramic stereolithography," in *IEEE MTT-S Int. Microwave Symp.*, (Honolulu, Hawaii, 2007), pp. 1431-1434.

#97423 - $15.00 USD Received 13 Jun 2008; revised 27 Sep 2008; accepted 28 Sep 2008; published 1 Oct 2008

17. N. Delhote, D. Baillargeat, S.Verdeyme, C. Delage, and C. Chaput, "Ceramic layer-by-layer stereolithography for the manufacturing of 3-D millimeter-wave filters," IEEE Trans. Microwave Theory Tech. **55**, 548-554 (2007).
18. Objet^{TM}, http://www.2objet.com/Default.aspx.
19. High Frequency Structure Simulator, Version 11, Ansoft Corporation, 2007.
20. Microwave Studio, Computer Simulation Technology, 2006.
21. Z. Wu, L. Wang, Y. Peng, A. Young, S. Seraphin, and H. Xin, "Terahertz characterization of multi-walled carbon nanotube (MWNT) films," J. Appl. Phys. **103**, 094324 1-6 (2008).
22. K. M. Ho, C. T. Chan, C. M. Soukoulis, C. M., R. Biswas, and M. Sigalas, "Photonic band gaps in three dimensions: new layer-by-layer periodic structures," Solid State Commun. **89**, 413-416 (1994).
23. S.Y. Lin, J. G. Fleming, D. L. Hetherington, B. K. Smith, R. Biswas, K. M. Ho, M. M. Sigalas, W. Zubrzycki, S. R. Kurtz, and Jim Bur, "A three-dimensional photonic crystal operating at infrared wavelengths," Nature **394**, 251-253 (1998).
24. P. U. Jepsen and B. M. Fischer, "Dynamic range in terahertz time-domain transmission and reflection spectroscopy," Opt. Lett. **30**, 29–31 (2005).
25. S. G. Johnson and J. D. Joannopoulos, "Three-dimensionally periodic dielectric layered structure with omnidirectional photonic band gap," Appl. Phys. Lett. **77**, 3490-3492 (2000).
26. M. Qi, E. Lidorikis, P. T. Rakich, S. G. Johnson, J. D. Joannopoulos, E. P. Ippen, and H. I. Smith, "A three-dimensional optical photonic crystal with designed point defects," Nature **429**, 538-542 (2004).

1. Introduction

Research involving the Terahertz (THz) spectrum (informally defined as 100 GHz—10 THz) has recently been experiencing rapid growth [1]. This growth is application-driven and involves wide-ranging topics including: chemical and astronomic spectroscopy and sensing [1], medical and biological imaging and analysis [2], defense and security screening [1], material research and semiconductor industry [3], and next generation communication networks and radars [4]. The great potential of THz technology originates from the plethora of physical and chemical processes occurring in this region as well as the relatively high resolution and bandwidth of THz compared with microwave frequencies. Additionally, free space THz communication suffers less scattering loss than free space optical communication, and is able to function under IR and optical blind conditions such as smoke, cloud and sandstorm. Recently, many THz applications have become closer to reality with the rapid advancing of THz sources, detectors and other novel components [1].

Electromagnetic bandgap (EBG) materials—materials in which certain propagating modes are forbidden—is currently one of the most rapidly advancing subfields in electromagnetic research. Because of their special nature, EBG structures can be used to control and tailor optical processes such as emission and detection of electromagnetic radiation [5]. Many works have been reported on EBG-based THz components, including sources, detectors, filters, waveguides and artificial dielectrics [1, 4, 6, 7]. However, one of the major challenges remaining to be overcome involves the practical difficulties in component fabrication, as the feature dimensions of THz EBG components fall in a transition region between the conventional micromachining techniques used for microwave applications and the micro/nano-fabrication methods in use at optical frequencies [8]. Several semiconductor fabrication approaches, including dicing saw machining [9], wet etching [10], deep reactive iron etching (DRIE) [11], deep X-ray lithography [12] and laser micromachining [8,12], have been reported. These methods are expensive, and require extraordinary care to achieve even relatively uniform THz EBG geometries, let alone the more complicated structures such as defect cavities and waveguides.

Alternatively, a variety of rapid prototyping technologies have been explored for fabricating 3-D microwave circuits and EBG components, including polymer and ceramic stereolithography [13, 14], fused deposition modeling [15] and selective laser sintering [15]. Among them, polymer stereolithography has the highest accuracy [14]. Using these methods, EBG waveguides [16], 3-D antennas [17] and band-pass filters [13] have been demonstrated. However, these techniques were only successful at frequencies up to approximately 30 GHz.

This manuscript represents a collaboration between two research groups at the University of Arizona—the primary result of which is the utilization of a new rapid prototyping

#97423 - $15.00 USD Received 13 Jun 2008; revised 27 Sep 2008; accepted 28 Sep 2008; published 1 Oct 2008

technology to achieve rapid and inexpensive fabrication of high-quality EBG structures in the THz range.

2. Fabrication technique

The multiple-scattering nature of EBG-physics requires that the EBG structure exhibit sub-wavelength features. For the frequency range of interest (100 GHz—10 THz), the corresponding wavelength range is 3 mm—30 μm. Of course, the particular constant of proportionality between a characteristic feature size and the wavelength at which the bandgap occurs depends critically on particular structure design. However, in general, to produce useful bandgap structures in this wavelength range, a fabrication technique that can provide feature sizes in the range 1mm—10 μm is required.

Polymer-jetting rapid prototyping machines now have build resolutions that fall in this range. The lab of one of the authors (MG) contains a commercial rapid prototyping machine (Objet Eden 350 [18]) that claims a fundamental resolution of 42 μm in the x and y directions and 16 μm in z direction.

For this prototyping machine, the fabrication process is relatively straightforward. The desired EBG structure is designed and analyzed in an electromagnetic simulation program such as HFSS [19] or CST [20]. Once the design is finalized, the resulting 3-D geometry is exported into a CAD program where it is converted into a series of layered slices, each representing a 16 μm-thick region of the model. As earlier slices provide the surface upon which later slices are constructed, the slice description consists of two different material types—a *model* material which is assigned to regions that are actually part of the cross-section of the desired object, and a *support* material, which is used to provide a base upon which the model sections of future slices can rest.

The data describing the slices are sent sequentially to the prototyping machine. As each slice arrives, a series of print heads, much like the print heads of an inkjet printer, deposit a thin layer of two different UV-curable materials onto the construction tray. Regions identified as model material in the slice are covered with uncured acrylic polymer, while support material regions receive uncured water-soluble polymer. UV lamps on the print head immediately cure both materials as they are being deposited. After the layer is complete, the construction tray is lowered by 16 μm and the next slice is processed.

After the entire model is complete, the construction tray rises and the part may be removed. For traditional rapid prototyping tasks, the finishing step involves using a high-pressure water spray to remove the water-soluble support material, leaving just the model material in the desired 3D shape.

Our initial attempts at constructing THz EBG structures via this approach revealed several areas where we needed to modify the standard fabrication methodology, or adapt certain limitations into our design process. First, despite the stated resolution of the machine (42 μm x 42 μm x 16 μm), we found that the minimum practical feature sizes in x and y are approximately 200 μm. Thus we limit our designs to these scales. Since this is a factor of 20 larger than the minimum desired feature size of 10 μm, to the first order, we expect our maximum frequency to scale inversely by the same factor. Thus, with this effective resolution, we should be able to produce fundamental bandgaps up to frequencies on the order of 500 GHz. Second, the resulting structures are far too fragile to withstand prolonged washing with the high pressure water jet. We find that soaking the part in a 3% aqueous solution of sodium hydroxide (NaOH) softens the support material to the point where it can be gently washed away.

Construction of THz EBG structures with this system is extremely quick and inexpensive. The time required to fabricate parts with the rapid prototyping machine is volume dependent (as this controls the size and number of slices that must be fabricated). For the EBG structures constructed to date (see next section), build times have been approximately 30 minutes, with consumable costs of approximately $10.

#97423 - $15.00 USD Received 13 Jun 2008; revised 27 Sep 2008; accepted 28 Sep 2008; published 1 Oct 2008

3. Experimental verification

To validate the fabrication technique, we designed and fabricated two different EBG structures and measured their transmission responses via a THz Time-domain spectrometer (THz-TDS) that is available to the research group of one of the authors (HX). The THz-TDS operates by propagating a picosecond-duration pulse through the material under test and Fourier transforming the time-domain transmission signal to extract the frequency content. The instrument has a spectral range of 50 GHz—1.2 THz with a maximum frequency resolution of 0.417 GHz. The results of the THz-TDS measurements were then compared to simulations of transmission properties of the structures.

3.1 Polymer characterization

For the design (and eventual simulation) of the structures, it became necessary to characterize the electromagnetic properties of the model polymer, specifically the complex permittivity ($\varepsilon = \varepsilon' - j\varepsilon''$) and permeability ($\mu = \mu' - j\mu''$). As the polymer is non-magnetic ($\mu = 1$), the complex permittivity was determined by performing a single transmission experiment using THz-TDS [21]. The dielectric constant ε' and the loss tangent $tan\delta = \varepsilon''/\varepsilon'$ (a convenient parameter representing loss of a dielectric material) were extracted from the measured magnitude and phase of the transmission coefficient of a uniform 3 mm thick slab of the polymer material.

As the fabrication process involved water and aqueous solutions as discussed in Section 2, sample dehydration might have been necessary to avoid the significant loss of THz signals in water [2]. To investigate the impact of water content in the polymer structures, the polymer slab was first characterized, and then placed in a desiccation chamber. Initially, the weight of the sample decreased as water was extracted, but eventually the weight stabilized, and the sample was removed. During this process we observed a weight decrease of approximately 0.5%. After desiccation, the slab characteristics were again measured and compared with the pre-desiccation results. In the 100—600 GHz spectral range, the loss tangent of the desiccated sample was smaller than the undesiccated sample, but the two differ by less than 30% (worst case and the differences for most frequencies are less than 20%). The dielectric constants in the two cases were almost identical. Therefore, we considered signal attenuation from the water content in the polymer as mild (would result in an additional transmission loss of ~ 1 dB), and did not desiccate the EBG structures before testing. The dielectric constant and loss tangent for the desiccated sample are plotted in Fig. 1. A slow decrease of the dielectric constant is observed as frequency increases, from 2.78 at 100 GHz to 2.7 at 600 GHz. The material loss tangent slowly increases from 0.02 around 100 GHz to 0.05 at 600 GHz.

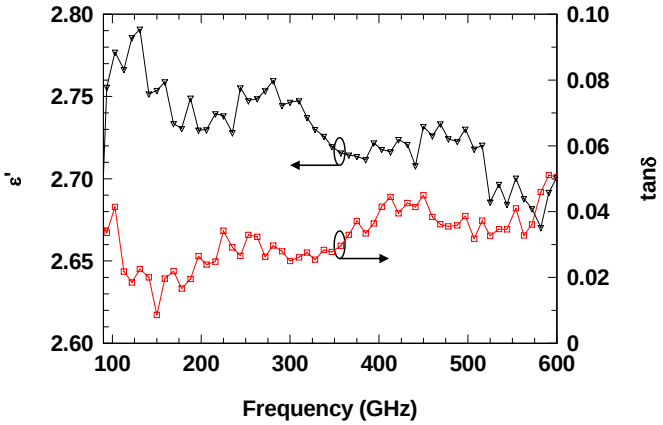

Fig. 1. Polymer slab THz characterization results. The real part of the permittivity ε' (open triangle) is plotted with left ordinate, and the loss tangent $\tan\delta$ (open rectangle) is plotted with right ordinate.

#97423 - $15.00 USD Received 13 Jun 2008; revised 27 Sep 2008; accepted 28 Sep 2008; published 1 Oct 2008

According to the above results, a refractive index ($n = \mathrm{Re}(\varepsilon^{1/2})$) contrast of around 1.66, with respect to the air background, is provided by the model material. With this refractive index contrast, periodic structures may exhibit EBG behaviors, although the bandgap will not be as wide as EBG structures made of materials with larger refractive index contrast such as silicon ($n \sim 3.6$). The reader should also note that there are several different polymer formulations available for this particular rapid-prototyping machine. The electromagnetic properties of the other materials are currently under test in our laboratories.

3.2 Woodpile structure example

The first EBG structure we tested was the well-known woodpile structure (WPS) with a complete 3D bandgap [22]. A schematic representation of the WPS is shown in Fig. 2(a) [23]. The structure consists of a unit cell containing 4 layers of infinitely long square rods, stacked with a periodicity D. Within the unit cell, the rods in each layer are distributed with the same periodicity d, and the adjacent layers that have the same rod orientation are shifted with respect to each other by d/2. Each rod has a height h = D/4 and a width w = h. Therefore, the filling ratio of the rods with respect to the whole structure is equal to w/d. The structure can be treated as a face-centered-tetragonal (fct) lattice with the unit cell being two attaching rods oriented in <1 1 0> and <1 $\bar{1}$ 0> lattice direction (see Fig. 2(a)). The center frequency of the WPS bandgap is scalable with its lattice parameters. By varying the filling ratio, the width of the bandgap can also be adjusted.

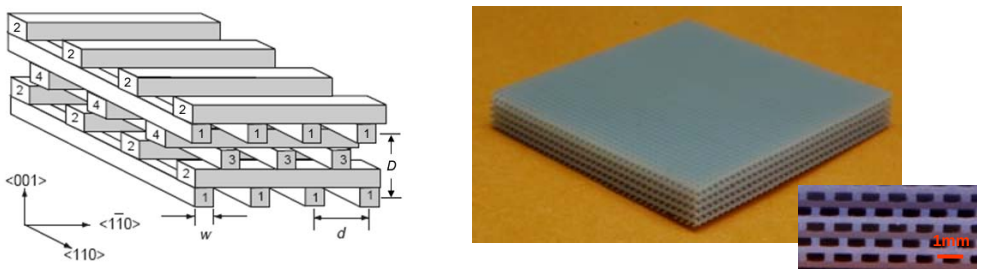

(a) (b)

Fig. 2. (a). A schematic drawing of the woodpile structure (from [23]). (b). Photographs of the fabricated polymer THz WPS. Inset is a zoomed-in view of the sample cross-section.

Using the previously-measured electromagnetic characteristics of the model material, we designed a WPS structure so that the bandgap is positioned at 185 GHz. Figure 2(b) shows a photograph of the fabricated polymer WPS. It has a rod dimension of w = h = 352 μm and a periodicity d = 1292 μm. In the stacking direction, it consists of 5 unit cells (20 layers of rods). The transverse area is sufficient to fully cover the incident beam of the THz-TDS. The inset of Fig. 2(b) is a zoomed-in view of the sample cross-section. Clean, sharp feature edges are clearly visible and match the structure shown in the schematic.

#97423 - $15.00 USD Received 13 Jun 2008; revised 27 Sep 2008; accepted 28 Sep 2008; published 1 Oct 2008

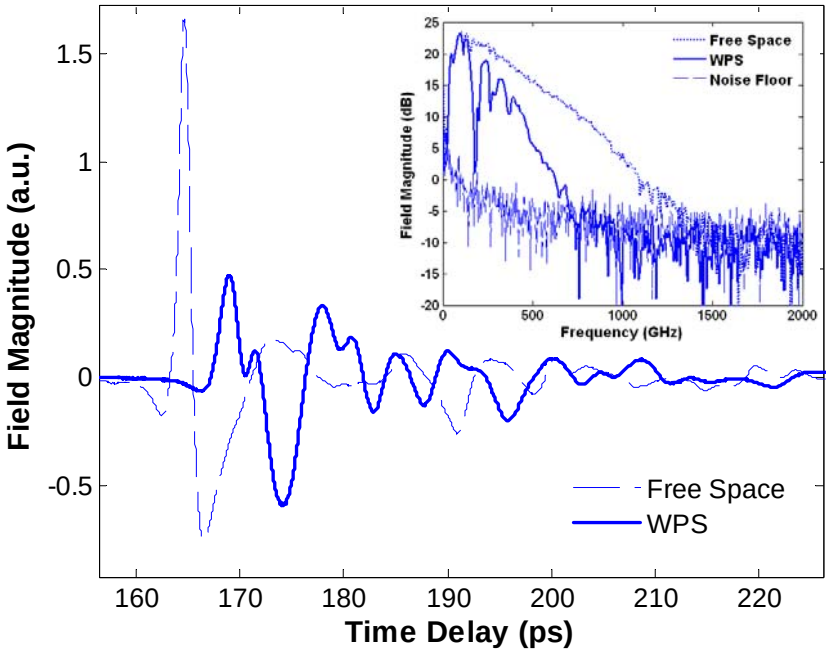

Fig. 3. THz-TDS measured free space signal waveform (dashed) and the WPS sample transmitted waveform (solid). Inset shows the frequency domain signals of the sample (solid), the free space (dotted), and the experiment noise floor (dashed).

The transmission response of the fabricated polymer WPS sample was then measured with the THz-TDS, with the incident energy propagating along the stacking direction (<001> in the schematic). The transmitted waveform is recorded and plotted as the solid line in the main portion of Fig. 3. The dashed line in the main portion of Fig. 3 is the time domain signal of the waveform through free space (with the EBG sample removed from the instrument). The decaying resonances introduced by the periodic structure of the WPS can be clearly seen. The inset of Fig. 3 plots the transmitted signal spectrum of the pulse through free space (dotted) and through the WPS (solid). In addition, the experiment noise floor (dashed) is also plotted. The noise floor was measured by completely blocking the incident pulse with a metal plate. The noise floor is important since it indicates the dynamic range and the usable frequency range of the measurement results [24]. From the measured sample transmission and noise level, the WPS sample response is valid from 50 GHz to 600 GHz.

The WPS power transmittance spectrum was obtained by taking the ratio of the frequency domain signals for the WPS and free space. It is plotted in Fig. 4. We see that the fabricated polymer WPS exhibits a fundamental EBG at around 180 GHz, with a band rejection of more than 35 dB. The secondary and tertiary bandgaps at 278 GHz and 372 GHz, respectively, are also observed in the measured power transmittance. Using -15 dB as the criteria of band edges, the sample has a main EBG bandwidth of 48 GHz. Its full bandwidth to mid-gap frequency ratio $\Delta f / f_0$ is therefore around 26.7%. The measured EBG performance qualifies this polymer WPS as a good band pass / stop filter.

As comparison to the measurement, the same WPS was simulated with the full-wave finite-element electromagnetic solver HFSS [19]. For the purposes of the simulation, the polymer material was modeled as a pure dielectric with $\varepsilon' = 2.76$ and $tan\delta = 0.06$. We used a loss tangent that is slightly higher than the maximum observed value of 0.05 (as shown in Fig. 1) so that the material loss would not be underestimated in the simulation. The WPS normal-incidence power transmittance from 100 GHz to 450 GHz is simulated and the result is also

#97423 - $15.00 USD Received 13 Jun 2008; revised 27 Sep 2008; accepted 28 Sep 2008; published 1 Oct 2008

plotted in Fig. 4 (solid line). We observe excellent agreement between measurement and simulation. Not only is the fundamental bandgap (centered at 185 GHz) verified, but a small resonance near 202 GHz can also be consistently seen in both the simulated and the measured results. Moreover, the simulated and measured secondary and tertiary bandgaps (centered at 278 GHz and 372 GHz, respectively) are in very good agreement in terms of location, width and depth. The small (< 2 dB) discrepancy of the transmission level at the low frequency end between the simulation and the measurement is a result of the overestimation of the material loss. As previously mentioned, the simulation assumed a loss tangent of 0.06, while the measured loss tangent near 100 GHz is approximately 0.02. The overall excellent consistency between the measurement and the simulation results confirms the fabrication accuracy of the polymer jetting technique.

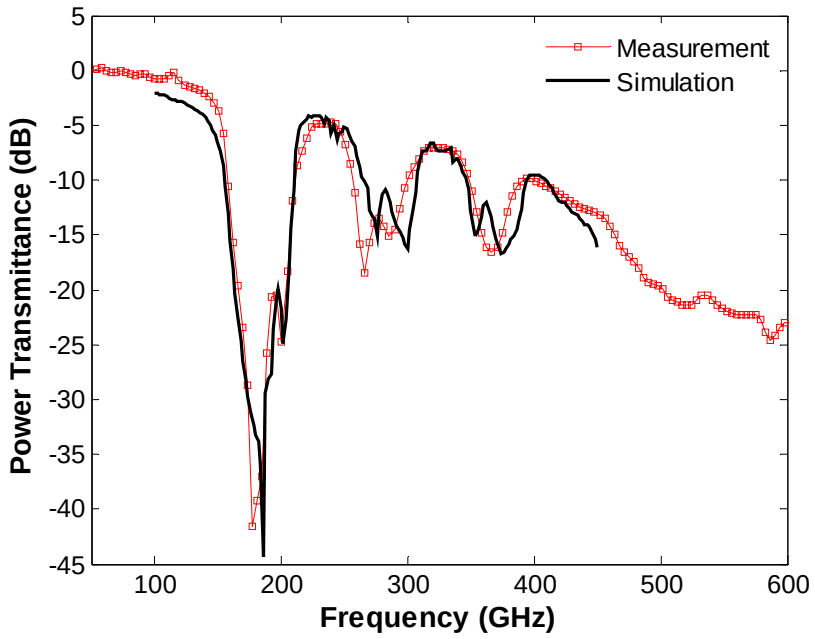

Fig. 4. Comparison between the measured (open squares) and simulated (solid line) WPS normal-incidence power transmittances.

3.3 Johnson structure example

The second EBG structure we tested was a more complicated three-dimensional bandgap structure first proposed by Johnson and Joannopoulos [25], and later fabricated by the same group [26]. We refer to this as the "Johnson-structure" (JS). A computer rendered structure model is shown in Fig. 5 (left). The structure consists of two alternating 2-D triangular lattice layers, one being pseudohexagonal dielectric pillars standing in air (rod layer) and the other being air holes in dielectric (hole layer). Each air hole has a radius r, and the size of each dielectric pillar is defined by the three surrounding air holes. The rod and hole layers have the same lattice constant x. The adjacent rod (hole) layers are shifted from each other by $x/\sqrt{3}$ in the x direction, thus forming the ABCA sequence in the stacking z direction as shown in Fig. 5 (lower right). The structure unit cell therefore includes three rod layers and three hole layers in the stacking direction. Figure 5 (upper right) shows the structure cross section: the height of the through air holes is h, and the height of two touching layers (one hole layer and one rod

#97423 - $15.00 USD Received 13 Jun 2008; revised 27 Sep 2008; accepted 28 Sep 2008; published 1 Oct 2008

layer) is t. The omnidirectional bandgap of this structure has a scalable center frequency with the above parameters, among which the air hole radius is the primary determinant of the gap bandwidth [8].

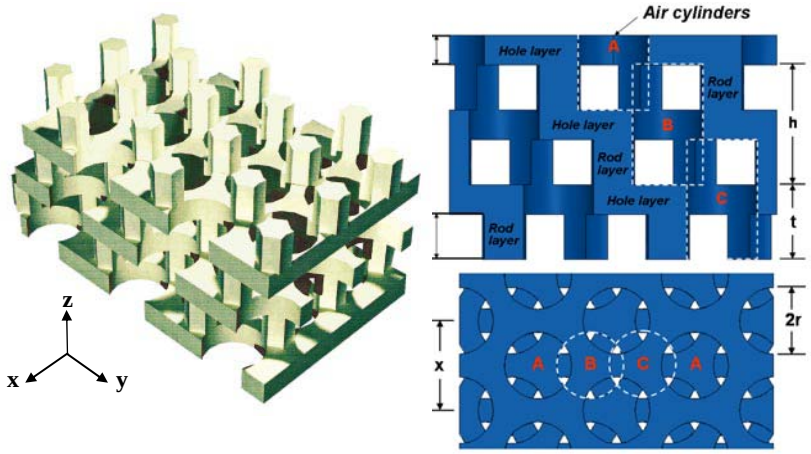

Fig. 5. Schematics of the Johnson EBG structure, including: a 3-D model (left) showing one unit cell in the stacking direction and several periods in the horizontal direction (from [25]), the cross-sectional view (upper right), and the top view (lower right).

In this work, we took the dimensions of the original fabricated sample (designed to work at optical frequencies [26]) and scaled them to THz region. The resulting THz JS has the following dimensions: triangular lattice constant x = 1346 μm, air hole radius r = 500 μm, air hole height h = 1713 μm, and rod / hole layer height t = 1071 μm. Based on the results in [26], the structure was expected to exhibit a complete bandgap around 200 GHz.

A photograph of the fabricated JS is shown in Fig. 6 (left). A top and a side microscopic view of the structure are also included in Fig. 6 (right). In the top view (lower right), the hexagonal air hole array is clearly defined, and lower shifted hole layers are observed. A design choice resulted in the posts having truly circular cross-sections, but this was not expected to dramatically impact the EM behavior of the structure [25]. The shifted adjacent rod layers were also correctly fabricated, as can be seen in the side view. Three unit cells including 9 hole layers and 9 rod layers in the stacking direction were fabricated, resulting in an overall EBG structure dimension of 25mm x 25mm x 9.6mm.

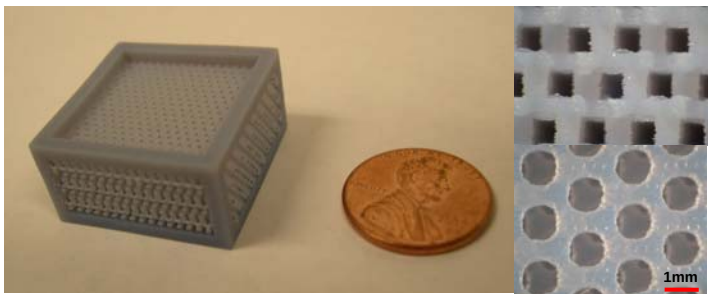

Fig. 6. Photographs of the fabricated polymer Johnson EBG structure, including: the full view (left), the side (cross-sectional) view (upper right), and the top view (lower right). Clearly defined air hole and dielectric rod layers are observed.

#97423 - $15.00 USD Received 13 Jun 2008; revised 27 Sep 2008; accepted 28 Sep 2008; published 1 Oct 2008

As the WPS structure, THz-TDS was used to measure the normal-incidence transmission properties of the JS. The sample power transmittance spectrum was measured and plotted in Fig. 7. A larger loss through this thicker sample (compared with the WPS) resulted in smaller transmitted signals. As a result, the noise floor becomes significant at frequencies above 350 GHz. As such, we limited our analysis to the 50—350 GHz region. A fundamental bandgap centered at 223 GHz is clearly observed, with a band rejection of around 25 dB, and a full bandwidth to mid-gap frequency ratio of 15.4%. The structure also exhibits a smaller transmission dip at 117 GHz, with band rejection of less than 15 dB. We have also investigated non-normal incidence (specifically, along the x-direction of Fig. 5). In this case, the measured transmittance (not shown) is very similar to the normal-incidence results, showing a 117 GHz transmission dip and the fundamental bandgap starting at around 200 GHz. This result partially confirms the expected isotropic property of the JS bandgap.

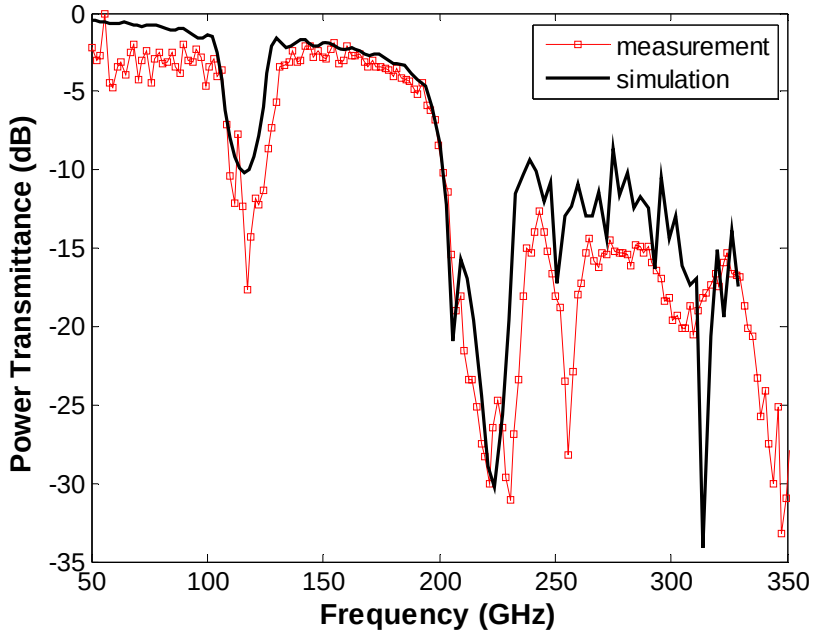

Fig. 7. Comparison between the measured (open squares) and simulated (solid line) Johnson structure normal-incidence power transmittances.

As before, we simulated the JS with HFSS. The solid curve in Fig. 7 shows the simulated normal-incidence, three-unit cell sample power transmittance from 50 GHz to 330 GHz. Both the mid-gap frequency and the gap rejection depth of the fundamental EBG around 220 GHz are verified. The secondary transmission dip around 120 GHz is also confirmed. Both gaps are slightly wider in the measurement than in the simulation, probably as a result of a small inhomogeneity of array pitches. The two additional transmission dips measured at 255 GHz and 309 GHz can also be matched to features in the simulated spectrum, although their correspondence is not as strong. The overall matching between the structure design and characterization is significant. This once again demonstrates the capability of the polymer jetting approach to handle complicated THz structures.

4. Conclusion and discussion

We have successfully used a polymer jetting technique to fabricate high-quality 3-D THz EBG structures. THz-TDS characterizations of the fabricated WPS and JS show extremely

#97423 - $15.00 USD Received 13 Jun 2008; revised 27 Sep 2008; accepted 28 Sep 2008; published 1 Oct 2008

good correspondence with the EM simulations, confirming the high dimensional accuracy and geometric complexity achievable with this fabrication technique. The speed, convenience, flexibility, and low-cost nature of the technique make this methodology highly promising for further THz EBG applications. We are currently working to reduce the effective resolution of the fabrication technique, thus allowing fabrication of bandgap structures at frequencies above 1THz.

Potential future capabilities resulting from this fabrication approach include: 1) Simultaneous fabrication of THz EBG components and the mounting structures; 2) inclusion of defects into the fabricated EBG structure; 3) metallic EBG component fabrication by metal deposition on molds fabricated via this technique; 4) Heterostructure fabrication of THz EBG materials. Further investigation of these techniques and related concepts are currently underway.

Acknowledgments

ZW and HX wish to thank Xiaoyan Tu for assistance with the sample desiccation and photography. JK and MG wish to thank Wei-Ren Ng for assistance with the creation of the 3D CAD models. The work of HX was supported in part by NSF Award 0823864.

#97423 - $15.00 USD Received 13 Jun 2008; revised 27 Sep 2008; accepted 28 Sep 2008; published 1 Oct 2008